Study of the angular correlation of the γ radiation emitted following beta decay

Group 25

Rocco Ardino Matr. 1231629
Francesco Gentile Matr. 1239149
Matteo De Tullio Matr. 1225015

5-10-11 December 2019

1 Objectives

- The measurement of the efficiency with a source of unknown activity.
- The measurement of the angular correlation of the gamma radiation.

2 Experimental apparatus

The experimental apparatus consisted of:

- Two detectors placed at different distances, d_1 and d_2, from a ^{60}Co source.
- A ^{241}Am source used in order to improve the calibration accuracy.
- A FAN-IN-FAN-OUT and a CFTD modules.
- A Tektronix TDS 1002B oscilloscope.

3 Introduction

In this experiment we considered the β^- decay of ^{60}Co which leads to an excited state of ^{60}Ni (2.505 MeV). It finally ends up to its ground state through the emission of two γ rays in cascade. These two γ rays are emitted as independent events, both related to the orientation of the spin of the nucleus, so it is expectable to register a certain *angular correlation* between their directions. If we fix the *first* γ ray direction (isotropic emission), the probability density of finding the *second* γ ray at a certain angle θ with respect to the first one is called **angular correlation function** $C(\theta)$. It is more convenient to compare its value to the one it assumes with the configuration $\theta = 90°$:

$$A(\theta) = \frac{C(\theta)}{C(90°)} = 1 + a\cos^2\theta + b\cos^4\theta \qquad \begin{cases} a = \frac{1}{8} \\ b = \frac{1}{24} \end{cases} \tag{1}$$

Our purpose was to prove the correctness of this theoretical relation and in doing this we had to demonstrate that there should be a connection between the emission directions of the two γ rays and the nucleus spin.

4 Electronics

The system has been set in such a way that the first detector, say D_1, was at a fixed position and the other one, D_2, could freely rotate around the source. The anode signal coming from the detectors was connected to a FAN-IN-FAN-OUT module to double the incoming signals, then one of its outputs was connected directly to the oscilloscope, while the other outputs to two CFTD modules. The CFTD thresholds were set at the minimum values such that the oscilloscope did not show the noise. The CFTD provides two different outputs: a **prompt signal** and a **delayed signal**, whose width and delay were settable. Hence one output of the FAN-IN-FAN-OUT was directly sent to the input 1 of the digitizer and one delayed signal from the CFTD to the Coincidence Unit in OR mode: this output signal has been used as the trigger for the digitizer acquisition.

5 Calibration of the detectors

5.1 Optimization of the resolution of the detector

In order to perform correctly the next measurements, an optimized energy resolution was required in order to be able to distinguish the peaks located in the high energies region of the spectrum. When it comes to resolution, the most influential parameter is the **long gate (LG)**, that is the duration of the integration window in acquisition.

Data Acquisition and Analysis We tested the resolution trend of the 1333 keV peak with increasing values of the long gate between 250 and 600 (acquiring 1 minute for each one with steps of 50). This peak was fitted with a gaussian plus a linear background. The results can be extracted from Table 1, from which it is possible to assert that the optimal resolution is obtained for a long gate value of 350. However, it assumes slightly higher values (5.25% for D_1 and 5.30% for D_2) than the optimal value range (4.60% - 5.00% of the FWHM).

	LG	$\boldsymbol{\mu}$ [a.u.]	$\boldsymbol{\sigma}$ [a.u.]	**FWHM** [a.u.]	**R** (%)
Detector D_1	250	4769.7 ± 0.6	109.6 ± 0.7	258.11 ± 1.65	5.41 ± 0.03
	300	4966.5 ± 0.5	110.7 ± 0.6	260.70 ± 1.41	5.25 ± 0.03
	350	5074.8 ± 0.6	115.2 ± 0.6	271.30 ± 1.41	5.35 ± 0.03
	400	5140.0 ± 0.6	118.5 ± 0.5	279.07 ± 1.18	5.43 ± 0.02
	450	5180.5 ± 0.7	123.0 ± 0.9	289.67 ± 2.12	5.59 ± 0.04
	500	5214.0 ± 0.6	123.4 ± 0.6	290.61 ± 1.41	5.57 ± 0.03
	550	5233.7 ± 0.7	130.1 ± 0.8	306.39 ± 1.88	5.85 ± 0.04
	600	5238.2 ± 0.7	130.8 ± 0.8	308.03 ± 1.88	5.88 ± 0.04
Detector D_2	250	5356.0 ± 1.0	121.0 ± 1.0	284.96 ± 2.35	5.32 ± 0.04
	300	5596.7 ± 1.1	129.8 ± 1.4	305.68 ± 3.29	5.46 ± 0.06
	350	5735.7 ± 1.0	129.2 ± 1.1	304.27 ± 2.59	5.30 ± 0.05
	400	5820.3 ± 1.1	133.0 ± 1.3	313.22 ± 3.06	5.38 ± 0.05
	450	5887.6 ± 1.0	134.6 ± 1.1	316.98 ± 2.59	5.38 ± 0.04
	500	5914.8 ± 1.2	142.2 ± 1.5	334.88 ± 3.53	5.66 ± 0.06
	550	5945.2 ± 1.1	143.4 ± 1.3	337.71 ± 3.06	5.68 ± 0.05
	600	5964.1 ± 1.0	141.1 ± 1.1	332.29 ± 2.59	5.57 ± 0.04

Table 1: Results for D_1 and D_2. For D_1 the minimum of resolution is 5.25%, for a long gate value of 300; for D_2 the minimum of resolution is 5.30%, for a long gate value of 350.

5.2 Statistics in gamma spectrum and measurement accuracy

We wanted to know how the accuracy in the measurements, and so the error on the centroid of the fitted peaks, changed along with the statistics in the spectrum. In practice, the error on the centroid μ was calculated for different times of acquisition. This analysis was accomplished by considering the events in the energy spectrum with a timestamp minor than the time of acquisition taken into account. Moreover, this operation was done for 8 time values, from 30 to 240 seconds, and only for the 1333 keV peak. The results are reported in Tables 2 and 3.

t [s]	$\boldsymbol{\mu}$ [a.u.]	$\boldsymbol{\sigma}$ [a.u.]	**R** (%)
30	5070.2 ± 0.9	119 ± 1	0.0553 ± 0.0005
60	5070.5 ± 0.6	118.7 ± 0.5	0.0551 ± 0.0002
90	5070.3 ± 0.5	119.1 ± 0.7	0.0553 ± 0.0003
120	5070.6 ± 0.4	119.2 ± 0.4	0.0553 ± 0.0002
150	5070.8 ± 0.4	118.7 ± 0.5	0.0551 ± 0.0002
180	5071.3 ± 0.3	118.8 ± 0.3	0.0552 ± 0.0001
210	5071.3 ± 0.3	118.7 ± 0.3	0.0551 ± 0.0001
240	5071.5 ± 0.3	118.6 ± 0.3	0.0551 ± 0.0001

Table 2: Gaussian fits results for 1333 keV peak at different times, for detector D_1.

t [s]	μ [a.u.]	σ [a.u.]	R (%)
30	5721 ± 1	144 ± 2	0.0593 ± 0.0006
60	5728 ± 1	135 ± 1	0.0557 ± 0.0004
90	5731.1 ± 0.8	133.1 ± 0.9	0.0547 ± 0.0004
120	5732.9 ± 0.7	132.5 ± 0.6	0.0544 ± 0.0003
150	5733.2 ± 0.6	132.5 ± 0.6	0.0544 ± 0.0002
180	5733.0 ± 0.6	132.6 ± 0.5	0.0545 ± 0.0002
210	5733.2 ± 0.5	132.9 ± 0.5	0.0546 ± 0.0002
240	5733.1 ± 0.5	132.7 ± 0.4	0.0545 ± 0.0002

Table 3: Gaussian fits results for 1333 keV peak at different times, for detector D_2.

It is clear from the results that the error on the centroids of the gaussian fits decreases when the statistics is bigger, namely when the number of events acquired increases.

5.3 Calibration

We were ready to acquire the ^{60}Co spectrum with both the two detectors.

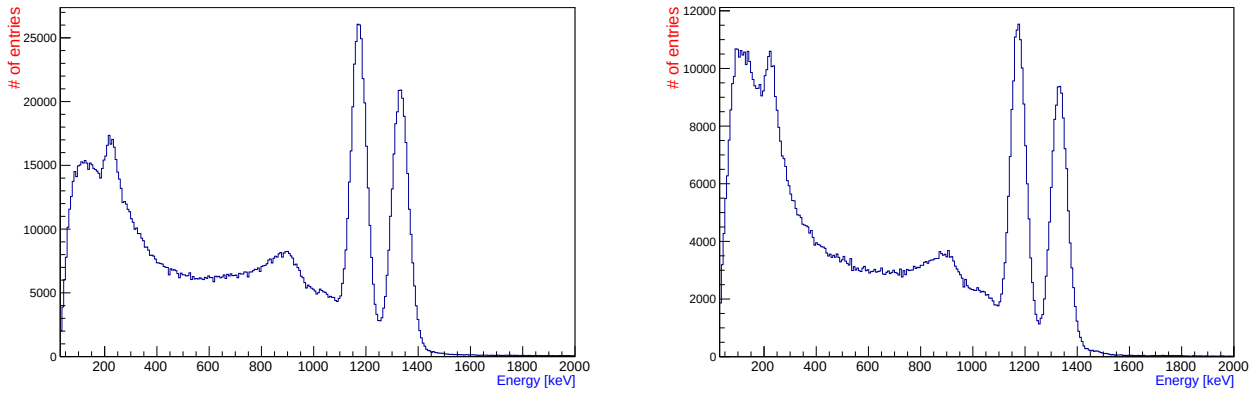

(a) *^{60}Co spectrum for detector D_1.* **(b)** *^{60}Co spectrum for detector D_2.*

Figure 1: ^{60}Co spectra obtained by the two detectors D_1 and D_2.

Spectrum description Increasing the energy it is possible to notice some noteworthy peaks. The clearest two to see, at 1173 and 1333 keV, represent the γ_1 and γ_2 energies completely stored in the detector. However, there is a portion of γ rays which experiences a Compton scattering before leaving the detector. The spectrum shows indeed two minor peaks, called *Compton edges* (one for each γ peak). Another evident peak can be noticed at lower energy (~ 250 keV). This one is nothing but an effect of *backscattering*, occurring when working with two detectors. When an incoming photon undergoes Compton scattering in one detector at such angle that the scattered photon ends up in the other detector, it is fully absorbed and so contributes to raise the peak.

Calibration To improve the accuracy of the calibration at low energies, we also used the 59 keV photo-peak of a ^{241}Am source. The procedure can be carried out for each detector in the following way: firstly it is necessary to fit the peaks with a gaussian curve plus a linear background to find the centroid values for each (μ_1, μ_2, μ_3) and then perform a linear fit of the

three points $(\mu_1, 59\text{ keV})$, $(\mu_2, 1173\text{ keV})$, $(\mu_3, 1333\text{ keV})$. The new calibrated values (energy in keV) can be extracted from the simple relation:

$$E_{\text{keV}} = a + b \cdot E_{\text{a.u.}} \qquad \begin{cases} a = \text{intercept} \\ b = \text{slope} \end{cases} \tag{2}$$

The results of the gaussian fits are reported in Table 4.

	$\mathbf{E}_{\text{th}}$ [keV]	$\boldsymbol{\mu}$ [a.u.]	$\boldsymbol{\sigma}$ [a.u.]	**FWHM** [a.u.]	**R** (%)
Detector D_1	59.5	251.0 ± 0.3	37.3 ± 0.5	88 ± 1	35.0 ± 0.5
	1173	4466.8 ± 0.3	109.3 ± 0.3	257 ± 1	5.76 ± 0.02
	1333	5069.4 ± 0.3	119.6 ± 0.2	281.7 ± 0.5	5.56 ± 0.01
Detector D_2	59.5	280.2 ± 0.1	43.3 ± 0.1	102.2 ± 0.2	36.4 ± 0.1
	1173	5058.7 ± 0.4	121.2 ± 0.4	285.4 ± 0.9	5.64 ± 0.02
	1333	5733.6 ± 0.5	131.9 ± 0.4	310.6 ± 0.9	5.42 ± 0.02

Table 4: Results of the gaussian fits for calibration for D_1 and D_2.

The values of the parameters obtained from the linear fit of the calibration are shown in Table 5.

Detector	**a** [keV]	**b** [keV/a.u.]
D_1	-6.86 ± 0.09	0.26425 ± 0.00002
D_2	-5.89 ± 0.02	0.23340 ± 0.00002

Table 5: Linear fit parameters related to the energy calibration for detectors D_1 and D_2.

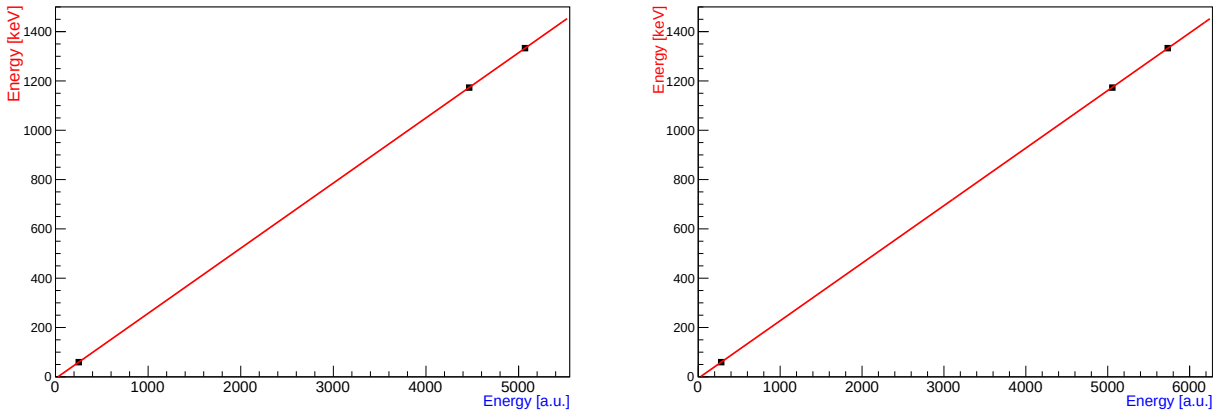

(a) *Detector D_1* **(b)** *Detector D_2*

Figure 2: Linear calibration for the two detectors D_1 and D_2, using ^{241}Am and ^{60}Co.

6 Evaluation of the Shift of the Source from the Rotation Axis

In this Section we are going to study the situation where the source is shifted from the rotation axis of the movable detector.

Geometry of the System We will briefly describe the geometry of the system and fix some notation. The distance of the movable detector from its rotation axis is $d_2 = 22$ cm, whereas the angle with respect to the rotation axis will assume the following values $\theta = 0°, 20°, 40°, 50°, 70°, 90°$. We are looking for the distance of the source form the rotation axis, which we will call y.

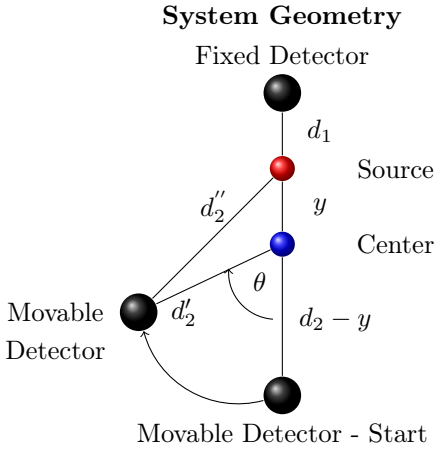

With some straightforward but rather long calculation, based on simple trigonometry, we can express the real distance of the movable detector from the source d_2'', as a function of y and θ:

$$(d_2'')^2 = (d_2)^2 + 2y^2(1 - \cos\theta) + 2d_2y(\cos\theta - 1) \tag{3}$$

Data Acquisition In the hypothesis of isotropic γ emission, the number of photons acquired by each detector in a fixed time interval, is proportional to the solid angle. Therefore, we have that:

$$\frac{1}{N} = K \cdot (d_2'')^2, \tag{4}$$

where K is an unknown proportionality constant. For such reason, we decided to acquire a γ spectrum in the angular positions $\theta = 0°$,$20°$, $40°$,$50°$,$70°$,$90°$, in a fixed time interval equal to 160 s. We show in Table 6 the number of counts acquired for each γ on the movable detector with the associated Poissonian error.

Angle [°]	**n° 1173 keV γ**	**n° 1333 keV γ**
0	66600 ± 200	61200 ± 200
20	64700 ± 200	59800 ± 200
40	65600 ± 200	61000 ± 200
50	65800 ± 200	61000 ± 200
70	65300 ± 200	60300 ± 200
90	65300 ± 200	61200 ± 200

Table 6: Photons acquired by the movable detector in a 160 s time interval

Data Analysis We assumed the following model:

$$\frac{1}{N} = K \cdot \left[(d_2)^2 + 2y^2(1 - \cos\theta) - 2d_2y(1 - \cos\theta)\right], \tag{5}$$

and fitted it using $(1 - \cos\theta)$ and $\frac{1}{N}$ as variables and K and y as the parameters to be fitted. The results of the fit are exposed in figure 3 and in table 7.

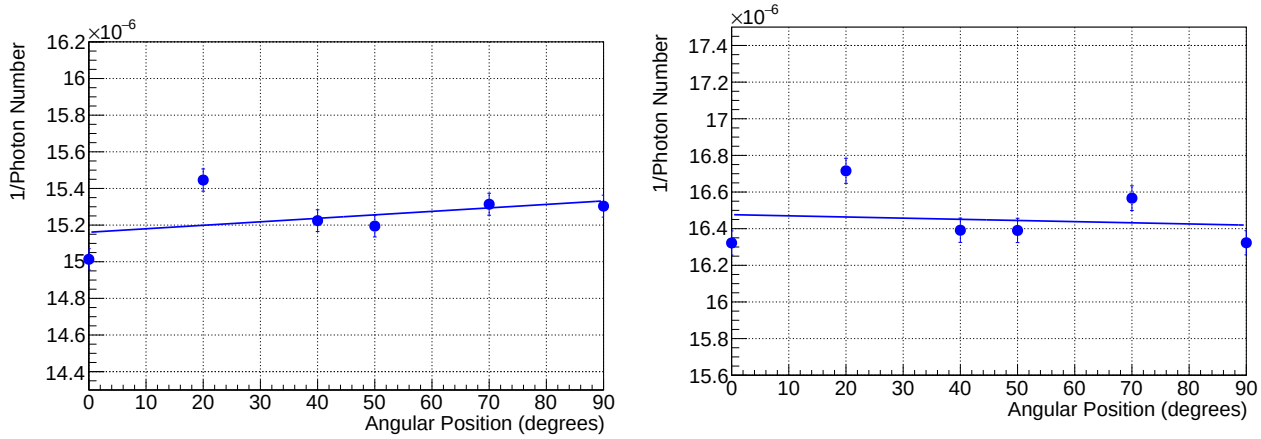

(a) *1173 keV γ ray* **(b)** *1333 keV γ ray*

Figure 3: Inverse of the number of γ as a function of the angular position.

	y [cm]	**K** [cm^{-2}]	$\boldsymbol{\chi^2}$**/d.o.f.**
1173 kev γ	$(3.132 \pm 0.009) \cdot 10^{-8}$	$(-1.3 \pm 0.6) \cdot 10^{-3}$	24/ 4
1333 kev γ	$(3.40 \pm 0.01) \cdot 10^{-8}$	$(4 \pm 6) \cdot 10^{-4}$	27/ 4

Table 7: Fit Parameters.

It is clear that the fit failed, leading us to reject the hypothesis that experimental data behave like the model in equation (3). Hence we can infer that, if there is a shift of the source from the rotation axis, this is not the most important and influential cause of the discrepancies observed in the number of photons acquired in each angular position. Observing the distribution of the dots in Figures 3a and 3b we can say that the number of photons acquired by the detector in each angular position is almost constant for $\theta = 40°, 50°, 70°, 90°$, whereas it has significant deviations for $\theta = 0°$ and $\theta = 20°$. The reason of this behaviour needs further investigation. It might be due to the anisotropy of the γ emissions or to a structural problem of the apparatus.

7 Measurement of the efficiency of detectors

The efficiency of detectors was measured in two different ways: the coincidence method and the sum peak method. The dataset analyzed was the same for both.

Data Acquisition The movable detector was fixed at the 0° position, while the electronics was set in the logic OR condition. The acquisition was splitted into 11 runs, each one 10 minutes long, for technical reasons. The output data of every run were merged and corrected by subtracting a properly scaled background spectrum.
The following notation will be employed for the sake of simplicity: $\varepsilon_{ij}^{\text{abs}}$ is the absolute efficiency of the detector D_j at the energy of γ_i. Hence:

$$\begin{aligned} i,j = 1 \ : \quad & \gamma_1 \sim \gamma_{1173 \text{ keV}} \quad & \text{D}_1 \sim \text{ch0} \\ i,j = 2 \ : \quad & \gamma_2 \sim \gamma_{1333 \text{ keV}} \quad & \text{D}_2 \sim \text{ch1} \end{aligned}$$

Note that the aim of this analysis is to calculate the efficiencies without relying on the activity value of the source.

7.1 Measurement of deadtime

Before the introduction of the two methods, the deadtime of the acquisition system should be calculated. In fact, in the analysis the background has to be subtracted from the energy spectra, but the deadtime while acquiring the background is negligible since the acquisition rate is very low. Therefore, the energy spectrum acquired with the source should be rescaled in order to take into account the non-negligible related deadtime.
For this purpose, a 3 minutes run was taken with the source inserted in the apparatus, with the OR logic condition, and two quatities were considered:

- N_{dgtz}: the number of counts registered by the digitizer.
- N_{scaler}: the number of counts registered by the CAEN scaler.

Their value for the 3 minutes run are:

$$N_{\text{dgtz}} = 1826000 \pm 1000$$
$$N_{\text{scaler}} = 1941000 \pm 1000$$

The deadtime rescaling factor was calculated through:

$$Q_{\text{deadtime}} = \frac{N_{\text{scaler}}}{N_{\text{dgtz}}} = 1.063 \pm 0.001 \tag{6}$$

The energy spectra in the following analysis were renormalized by this factor before subtracting a properly scaled background.

7.2 Coincidence method

For this method, we focused on the coincidences between D_1 and D_2, namely when in the same event D_1 detects γ_1 and D_2 detects γ_2, or viceversa. The counts of the former is denoted by C_1, the counts of the latter by C_2. The total counts of γ_i detected by D_j is denoted by N_{ij}. Then, by denoting the unknown activity of the source by A, we could compute the absolute efficiencies through:

$$\frac{C_1}{N_{22}} = \frac{\varepsilon_{11}^{\text{abs}} \varepsilon_{22}^{\text{abs}} A}{\varepsilon_{22}^{\text{abs}} A} = \varepsilon_{11}^{\text{abs}} \tag{7a}$$
$$\frac{C_1}{N_{11}} = \frac{\varepsilon_{11}^{\text{abs}} \varepsilon_{22}^{\text{abs}} A}{\varepsilon_{11}^{\text{abs}} A} = \varepsilon_{22}^{\text{abs}} \tag{7b}$$
$$\frac{C_2}{N_{12}} = \frac{\varepsilon_{21}^{\text{abs}} \varepsilon_{12}^{\text{abs}} A}{\varepsilon_{12}^{\text{abs}} A} = \varepsilon_{21}^{\text{abs}} \tag{7c}$$
$$\frac{C_2}{N_{21}} = \frac{\varepsilon_{21}^{\text{abs}} \varepsilon_{12}^{\text{abs}} A}{\varepsilon_{21}^{\text{abs}} A} = \varepsilon_{12}^{\text{abs}} \tag{7d}$$

The intrinsic efficiency is derived from the absolute one by dividing by the geometric factor G_j, which is calculated through the solid angle covered by the detector D_j at a distance d_j from the source:

$$G_j = \frac{1}{4\pi}\frac{\pi r^2}{d_j^2} \tag{8}$$

$$\varepsilon_{ij}^{\text{int}} = \frac{\varepsilon_{ij}^{\text{abs}}}{G_j} \tag{9}$$

where r is the radius of the detector.

7.3 Sum peak method

From the energy spectra, it is possible to distinguish a peak near 2506 keV, due to a relatively high probability to find both γ_1 and γ_2 in the same detector. This is called *sum peak* and its counts P_1 for D_1 and P_2 for D_2 can be exploited to compute the absolute efficiencies.
The procedure is not so different from the previous method. By keeping the same notation, the efficiencies can be computed through:

$$\frac{P_1}{N_{21}} = \frac{\varepsilon_{11}^{\text{abs}}\varepsilon_{21}^{\text{abs}}A}{\varepsilon_{21}^{\text{abs}}A} = \varepsilon_{11}^{\text{abs}} \tag{10a}$$

$$\frac{P_2}{N_{12}} = \frac{\varepsilon_{22}^{\text{abs}}\varepsilon_{12}^{\text{abs}}A}{\varepsilon_{12}^{\text{abs}}A} = \varepsilon_{22}^{\text{abs}} \tag{10b}$$

$$\frac{P_1}{N_{11}} = \frac{\varepsilon_{11}^{\text{abs}}\varepsilon_{21}^{\text{abs}}A}{\varepsilon_{11}^{\text{abs}}A} = \varepsilon_{21}^{\text{abs}} \tag{10c}$$

$$\frac{P_2}{N_{22}} = \frac{\varepsilon_{12}^{\text{abs}}\varepsilon_{22}^{\text{abs}}A}{\varepsilon_{22}^{\text{abs}}A} = \varepsilon_{12}^{\text{abs}} \tag{10d}$$

The intrinsic efficiency is computed in the same way as before, through Eq. 9.

7.4 Results

Practically, for the coincidence method we had to analyze the root files by selecting the events with the same timestamp and satisfying the coincidence condition previously defined. For the second method, we had to select the events near 2506 keV for both channels.
The number of counts for the quantities previously defined are presented in Table 8, the absolute and intrinsic efficiencies in Table 9 and 10. Note that background was subtracted after the calibration of the spectra.

	$\boldsymbol{E_\gamma}$ [keV]	**Detector**	**Counts**
N_{11}	1173	D_1	6547000 ± 3000
N_{12}	1173	D_2	2872000 ± 2000
N_{21}	1333	D_1	5957000 ± 2000
N_{22}	1333	D_2	2563000 ± 2000
C_1	$1173 \wedge 1333$	$D_1 \wedge D_2$	19200 ± 100
C_2	$1173 \wedge 1333$	$D_2 \wedge D_1$	19300 ± 100
P_1	$1173 + 1333$	D_1	39900 ± 200
P_2	$1173 + 1333$	D_2	13000 ± 100

Table 8: Number of counts for the coincidence and sum peak method.

Method:	Coincidence	Sum peak	λ
$\varepsilon_{11}^{\text{abs}}$	0.00750 ± 0.00005	0.00670 ± 0.00003	13.7
$\varepsilon_{12}^{\text{abs}}$	0.00325 ± 0.00002	0.00506 ± 0.00005	33.6
$\varepsilon_{21}^{\text{abs}}$	0.00673 ± 0.00005	0.00609 ± 0.00003	11.0
$\varepsilon_{22}^{\text{abs}}$	0.00294 ± 0.00002	0.00452 ± 0.00004	35.3

Table 9: Absolute efficiencies for the coincidence and sum peak methods and compatibility.

Method:	Coincidence	Sum peak	λ
$\varepsilon_{11}^{\text{int}}$	0.307 ± 0.002	0.274 ± 0.001	13.7
$\varepsilon_{12}^{\text{int}}$	0.447 ± 0.003	0.697 ± 0.006	33.6
$\varepsilon_{21}^{\text{int}}$	0.276 ± 0.002	0.250 ± 0.001	11.0
$\varepsilon_{22}^{\text{int}}$	0.404 ± 0.003	0.622 ± 0.005	35.3

Table 10: Intrinsic efficiencies for the coincidence and sum peak methods and compatibility.

Discussion The results of the two methods are incompatible. An explanation can be that a significative systematic error coming from false coincidences was not taken into account for the coincidence method. In principle, to get a better result, a count of false coincidences should be subtracted to the true coincidences, i.e. the ones coming from the same decaying nucleus. In fact, it could happen that two different nuclei decaying approximately at the same time emit respectively a γ_1 and a γ_2, detected by D_1 and D_2 in coincidence. This phenomenon leads to the overestimation of the efficiencies computed through the coincidence method.
It is possible to estimate approximately the number of false coincidences through Monte Carlo techniques, so to improve the results obtained a simulation of the system should be done.
Moreover, it is important to denote for the sum method that another two sum peaks should be visible: 2346 e 2665 keV peaks, determined respectively by the detection of two γ_1 and two γ_2, coming from different nuclei, by the same detector. However, the precision of our apparatus was not sufficient to distinguish in the spectrum these peaks from the 2506 keV peak, introducing a systematic error for the sum peak method, and so an overestimation of the related efficiencies.
In conclusion, the results show that the order of magnitude of the efficiencies, from sum peak and coincidence method, is the same. Therefore, although the incompatibility, we consider this result satisfying and as just explained, it can be improved through the exclusion of the events involving the emission of γs from different decaying nuclei.

8 Measurement of the angular correlation

Finally, we tried to measure the angular distribution of photons and see whether our experimental estimates for $A(\theta)$ matched with the theoretical model described in equation (1).

Data Acquisition We placed the movable and the fixed detectors at two different distances from the source:

$$L_{\text{fixed}} = 12 \text{ cm} \quad L_{\text{movable}} = 22 \text{ cm} \tag{11}$$

We chose the following angular positions for the movable detector:

$$\theta = 0°, 20°, 40°, 50°, 70°, 90°, \tag{12}$$

and acquired the γ spectrum in coincidence with γ rays hitting the fixed detector. In both spectra, even if there was some noise, we could clearly distinguish the photopeaks corresponding to the γ emissions at 1173 keV and 1333 keV.

Data Analysis We considered two different types of signal:

- **Type 1 signals**, having a 1173 keV γ in the fixed detector and a 1333 keV γ in the movable detector.
- **Type 2 signals**, having a 1333 keV γ in the fixed detector and a 1173 keV γ in the movable detector.

In our analysis, we decided to keep separate the two datasets, because they had been acquired in slightly different conditions. First, we checked if the signals acquired were truly in coincidence. We decided to keep only type 1 and type 2 signals whose photons had the same timetag in both detectors. Such procedure led to the rejection of many events and made us sure that in both datasets we had all and only signals corresponding to the two ^{60}Co γ rays acquired in coincidence. Once the signal selection had been done, we counted how many signals were acquired in each angular position and dataset. We considered the acquisition of a type 1 or type 2 signal as a Poisson event and computed the statistical error on the signal number as the square root of the number of counts. Then, we normalized the number of counts in each angular position, to the counts obtained for $\theta = 90°$, in order to get an estimate for the quantity $A(\theta)$ in equation (1).

Results In Table 11 our experimental estimates for $A(\theta)$ are exposed and compared to the expected values through the gaussian compatibility test. It can be seen that both datasets give us predictions which are compatible with the theoretical value within a distance of 2σ.

$A(\theta)_{\mathrm{exp}}$ - Dataset 1	$A(\theta)_{\mathrm{exp}}$ - Dataset 2	$A(\theta)_{\mathrm{th}}$	λ - Dataset 1	λ - Dataset 2
1.22 ± 0.03	1.16 ± 0.03	1.17	1.8	0.2
1.16 ± 0.03	1.11 ± 0.03	1.14	0.7	1.2
1.10 ± 0.03	1.08 ± 0.03	1.09	0.3	0.4
1.09 ± 0.03	1.07 ± 0.03	1.06	1.3	0.5
1.07 ± 0.03	1.01 ± 0.02	1.02	2.0	0.03
1.00 ± 0.02	1.00 ± 0.02	1.00	0.0	0.0

Table 11: $A(\theta)$: Experimental Estimates *vs* Theoretical Values.

Figure 4a shows the theoretical distribution of $A(\theta)$ and those obtained fitting the function in Eq. 1 for each of the two datasets. Figure 4, instead, shows the residuals with respect to the theoretically expected values, normalised to the error associated to the experimental point:

$$\mathrm{NormRes} = \frac{A(\theta)_{\mathrm{exp}} - A(\theta)_{\mathrm{th}}}{\sigma_{A(\theta)_{\mathrm{exp}}}}. \tag{13}$$

It is clear that such residuals are not compatible with statistical fluctuations, because the experimental values are all overestimated for type 1 dataset or underestimated for type 2 dataset. Therefore, there is a systematical error, which looking at plot in Figure 4a seems to be a scaling error. The impact of such an error is really small because experimental points are no further than 2σ from expected values.

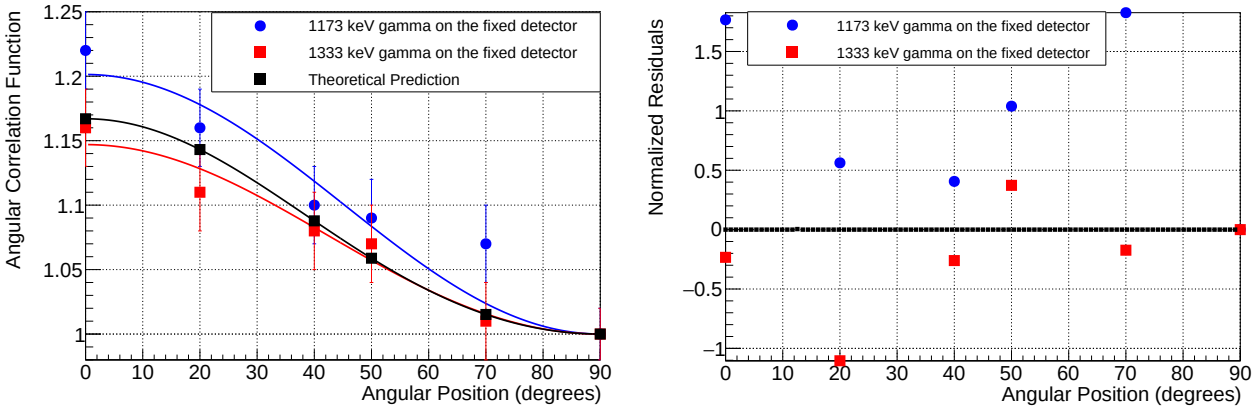

(a) *Experimental Prediction vs Experimental Values* **(b)** *NormRes with respect to Th. Expected Values*

Figure 4: Study of the Angular Correlation function $A(\theta)$.

	a	$\boldsymbol{\lambda_{th}}$	**b**	$\boldsymbol{\lambda_{th}}$	$\boldsymbol{\chi^2}$**/d.o.f.**
Dataset 1	0.20 ± 0.09	0.8	$0.0 \pm 0{,}1$	0.4	3.5 / 4
Dataset 2	0.13 ± 0.09	0.05	$0.0 \pm 0{,}1$	0.4	0.8 / 4
Theory	0.125	**	0.042	**	**

Table 12: $A(\theta)$: Fitted Parameters *vs* Theoretical Values.

As we can see from Table 12, the fit procedure made on both datasets is carried out correctly and give estimates for the parameters which are compatible with theoretical values. Some problems occur when we try to find the parameter b: the only information we get is that it is almost 0. This points out the necessity to enrich our datasets in order to get a more precise estimate of b.

9 Conclusion

We managed to give an estimate of the order of magnitude of the efficiency of the detectors using a source of unknown activity. The fact that the two different estimates, even if they are of the same order of magnitude, are not compatible points out that the methods need to be improved, including the correction of systematic errors.
Concerning the angular distribution, its reconstruction gave acceptable results. Experimental values are greatly compatible to theoretical expectations and also the fit parameters are compatible with theoretical values. It is evident the presence of a systematical error which acts with a different sign in the two cases considered: further investigations are needed. However the impact of this systematical error on experimental estimates is very little and does not affect the compatibility of theory with experiment.